AD-A057 967 DAYTON UNIV OHIO RESEARCH INST F/G 11/4
THE CHARPY IMPACT TEST AS A METHOD FOR EVALUATING IMPACT RESIST--ETC(U)
APR 78 D C KRINKE, J P BARBER, T NICHOLAS F33615-76-C-5124
UNCLASSIFIED UDRI-TR-77-54 AFML-TR-78-54 NL

| OF |
AD
A057967

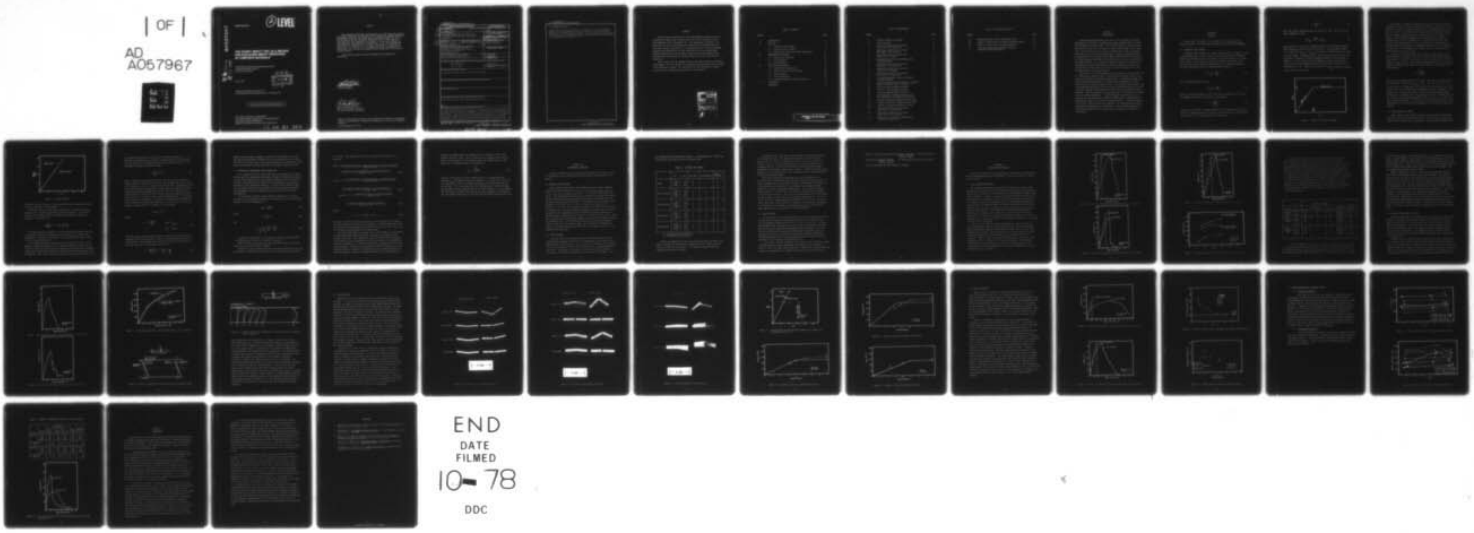

END
DATE
FILMED
10-78
DDC

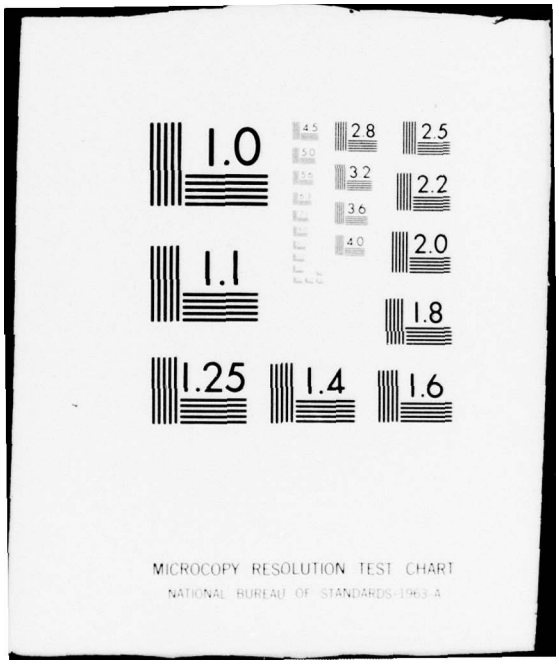
1.0
1.1
1.25
1.4
1.6
1.8
2.0
2.2
2.5
2.8
3.2
3.6
4.0
4.5
5.0
5.6
MICROCOPY RESOLUTION TEST CHART
NATIONAL BUREAU OF STANDARDS-1963-A

AFML-TR-78-54

(2) LEVEL II

THE CHARPY IMPACT TEST AS A METHOD FOR EVALUATING IMPACT RESISTANCE OF COMPOSITE MATERIALS

UNIVERSITY OF DAYTON RESEARCH INSTITUTE
300 COLLEGE PARK AVENUE
DAYTON, OHIO 45469

APRIL 1978

TECHNICAL REPORT AFML-TR-78-54
Technical Report for Period September 1976 – September 1977

Approved for public release; distribution unlimited.

AIR FORCE MATERIALS LABORATORY
AIR FORCE WRIGHT AERONAUTICAL LABORATORIES
AIR FORCE SYSTEMS COMMAND
WRIGHT-PATTERSON AIR FORCE BASE, OHIO 45433

NOTICE

When Government drawings, specifications, or other data are used for any purpose other than in connection with a definitely related Government procurement operation, the United States Government thereby incurs no responsibility nor any obligation whatsoever; and the fact that the Government may have formulated, furnished, or in any way supplied the said drawings, specifications, or other data, is not to be regarded by implication or otherwise as in any manner licensing the holder or any other person or corporation, or conveying any rights or permission to manufacture, use, or sell any patented invention that may in any way be related thereto.

This technical report has been reviewed and is approved for publication.

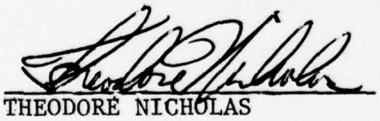

THEODORE NICHOLAS
Project Engineer

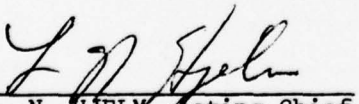

L. N. HJELM, Acting Chief
Metals Behavior Branch
Metals and Ceramics Division
Air Force Materials Laboratory

Copies of this report should not be returned unless return is required by security considerations, contractual obligations, or notice on a specific document.

AIR FORCE/56780/28 June 1978 — 300

UNCLASSIFIED

SECURITY CLASSIFICATION OF THIS PAGE (When Data Entered)

REPORT DOCUMENTATION PAGE

READ INSTRUCTIONS BEFORE COMPLETING FORM

1. REPORT NUMBER: AFML-TR-78-54	2. GOVT ACCESSION NO.
3. RECIPIENT'S CATALOG NUMBER	
4. TITLE (and Subtitle): THE CHARPY IMPACT TEST AS A METHOD FOR EVALUATING IMPACT RESISTANCE OF COMPOSITE MATERIALS.	5. TYPE OF REPORT & PERIOD COVERED: Technical Report, September 1976-September 1977
	6. PERFORMING ORG. REPORT NUMBER: UDRI-TR-77-54
7. AUTHOR(s): Mr. Dennis C. Krinke, Dr. John P. Barber, University of Dayton Research Institute; Dr. Theodore Nicholas, Air Force Materials Lab	8. CONTRACT OR GRANT NUMBER(s): F33615-76-C-5124
9. PERFORMING ORGANIZATION NAME AND ADDRESS: University of Dayton Research Institute, 300 College Park Avenue, Dayton, Ohio 45469	10. PROGRAM ELEMENT, PROJECT, TASK AREA & WORK UNIT NUMBERS
11. CONTROLLING OFFICE NAME AND ADDRESS: Air Force Materials Laboratory/LLN, Wright-Patterson Air Force Base, Ohio 45433	12. REPORT DATE: April 1978
	13. NUMBER OF PAGES: 36
14. MONITORING AGENCY NAME & ADDRESS (if different from Controlling Office)	15. SECURITY CLASS. (of this report): UNCLASSIFIED
	15a. DECLASSIFICATION/DOWNGRADING SCHEDULE

16. DISTRIBUTION STATEMENT (of this Report)

Approved for public release; distribution unlimited.

17. DISTRIBUTION STATEMENT (of the abstract entered in Block 20, if different from Report)

18. SUPPLEMENTARY NOTES

19. KEY WORDS (Continue on reverse side if necessary and identify by block number)

Composites, Foreign Object Damage, Charpy Impact Test

20. ABSTRACT (Continue on reverse side if necessary and identify by block number)

A detailed analysis of the three point bend (Charpy Impact) test was conducted. A simple strength of materials approach to the prediction of specimen response was extended to include shear deformation, shear yielding and local loading tup deformation. Load-deflection, energy absorbed and failure modes were predicted for graphite-epoxy, and two types of boron-aluminum composites. Experiments were then conducted on these materials and the observations compared to the predictions. The analysis was unable to predict specimen response accurately, especially when significant shear deformation or yielding occurred.

DD FORM 1 JAN 73 1473 EDITION OF 1 NOV 65 IS OBSOLETE

UNCLASSIFIED.

SECURITY CLASSIFICATION OF THIS PAGE (When Data Entered)

20. ABSTRACT (cont'd)

Loading point stresses were shown to be important. The energy absorbing capability of the specimen was shown to be geometry sensitive and highly dependent on the mode of failure induced. It was concluded that application of the bend test as a materials evaluation procedure requires careful analysis and interpretation of test results.

FOREWORD

This work was conducted for the Air Force Materials Laboratory by the University of Dayton under Contract F33615-76-C-5124, during the period from September 1976 to September 1977. The program was conducted in the facilities of the Air Force Materials Laboratory at Wright-Patterson Air Force Base and was monitored by Dr. Theodore Nicholas. The boron-aluminum materials were supplied by Dr. Karl Prewo from the United Technologies Research Laboratories, East Hartford, Connecticut and the graphite-epoxy specimens were prepared by Mr. George Hussman at the Air Force Materials Laboratory.

Direct support for the program from the following persons is gratefully acknowledged. Mr. Dick Klinger of the Systems Research Laboratories assisted in the mechanical testing. Mr. Bob Bertke from the University of Dayton assisted in the preparation and editing of the manuscript.

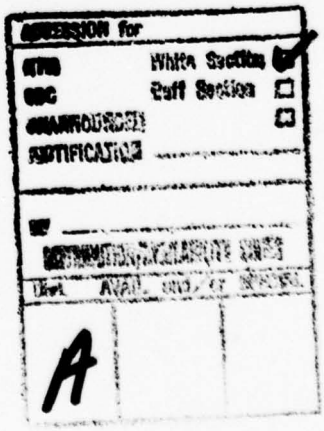

TABLE OF CONTENTS

LIST OF ILLUSTRATIONS

LIST OF ILLUSTRATIONS (CONT'D)

SECTION I
INTRODUCTION

Advanced composite materials have come to be recognized as primary candidates for fan blades in advanced jet engine designs because of their high strength to density ratios. The primary drawback to their potential application has been poor resistance to impact from foreign object ingestion. There has been little success in predicting, a priori, the impact resistance of a full stage or single blade. Finding a screening test(s) for evaluation of the foreign object damage (FOD) resistance of potential fan blade materials (both metals and composites) is, thus, a major goal of the engine industry. The three point bend, or Charpy test has been used extensively for evaluating candidate composite materials, although the interpretation of test results in terms of blade performance is not well established and raises many questions.

The purpose of this investigation was to evaluate the Charpy bend test for fiber-matrix composites and to determine what phenomena could be predicted from analysis and uniaxial tensile data. Instrumented Charpy tests were conducted (measuring the load-deflection relationship) at various deflection rates from slow-bend to those of the standard Charpy impact test. Boron-aluminum specimens of both 1100 and 6061 aluminum matrix were tested in several available thicknesses which were thinner than standard Charpy geometry. Tests on graphite-epoxy specimens were also conducted to compare with the boron-aluminum data. Several different thicknesses of each material were investigated to observe the differences in phenomena due to variation in length to thickness (slenderness) ratio. A detailed analysis of the three point bend test was conducted. The experimentally observed phenomena were compared with the analysis. There was some agreement and several discrepancies in the results which are discussed in detail in this report.

SECTION II
ANALYSIS

Several levels of analysis were applied to the three point bend (Charpy) specimen. The results are described in the following paragraphs.

2.1 ELEMENTARY BEAM FORMULAS

Elementary beam formulas for a simply supported beam of length, s, with a concentrated load, P, at the center can be used to predict the maximum stresses and deflections when the material of the beam behaves in a linear elastic manner. The strength of materials formulas which assume that plane sections remain plane and perpendicular to the deformed centerline (no shear deformation) give the maximum bending stress as;

$$(\sigma_x)_{max} = \frac{3Ps}{2wd^2} , \tag{1}$$

and the maximum shear stress as;

$$(\tau_{xy})_{max} = \frac{3P}{4wd} , \tag{2}$$

where w is the beam width and d the total depth (thickness) of the beam. The maximum deflection at the center of the beam is;

$$\delta = \frac{Ps^3}{4wd^3E_x} , \tag{3}$$

where E_x is the elastic or Young's modulus in the direction of the axis of the beam. Maximum strain rate occurs at the outer fibers at the center of the span and, for a deflection rate $\dot{\delta}$, is given by;

$$\dot{\varepsilon} \simeq \frac{6d}{s^2}\ \dot{\delta}\ , \tag{4}$$

where dots denote differentiation with respect to time. Eqs. (1) and (2) can be combined to give;

$$(\sigma_x)_{max} = 2\left(\frac{s}{d}\right)(\tau_{xy})_{max}\ , \tag{5}$$

which shows that the ratio of maximum bending stress to maximum shearing stress depends on the span to depth ratio s/d. For long slender beams (i.e. large s/d) $(\sigma_x)_{max} >> (\tau_{xy})_{max}$ and failure is governed by the ultimate bending strength. The variation σ_x at failure with slenderness ratio can be shown in a flexural interaction diagram (Reference 1) as presented in Figure 1. Up to a critical s/d, the maximum σ_x reached in the beam is limited by the shear strength and this value increases linearly with s/d according to Eg. (5). Beyond the critical s/d, $(\sigma_x)_{max}$ equals the ultimate tensile stress (in bending).

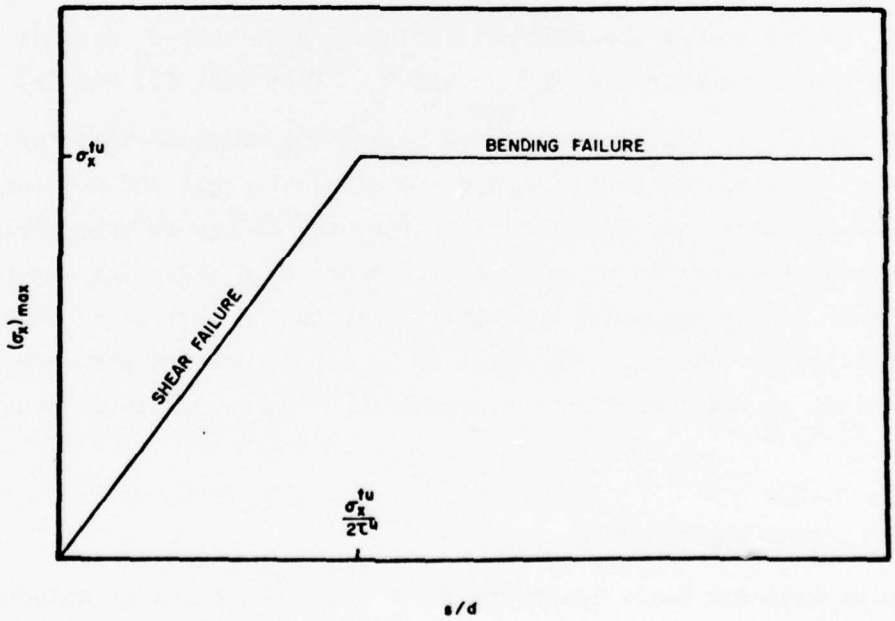

Figure 1. Flexural interaction diagram.

The failure of a beam thus depends not only on the ratio of ultimate strength in tension to that in shear but on slenderness ratio s/d. Eq. (5) shows that the ratio of maximum tensile stress to maximum shear stress in a beam is 2 (s/d). If the ratio of ultimate strengths in tension to shear for all materials is plotted against slenderness ratio for beams to be tested, a failure regimes diagram can be constructed as in Figure 2. A straight line of slope 2 represents all points where tensile and shear failure occur simultaneously. If s/d is decreased or shear strength is decreased (upper left direction on diagram) shear failure will occur first. The other part of the diagram (lower right) represents the region where bending failure will occur first.

A measure of the beams resistance to impact is often taken as the energy absorbed in a Charpy impact test. For an unnotched beam, which is linear elastic to failure, the energy to failure is given by one-half the product of P_{max} and δ_{max}. The energy absorbing capability of a material is commonly expressed as the energy to failure divided by the volume of the beam tested or;

$$U_o = \frac{(\sigma_x)^2_{max}}{18\ E_x}, \qquad (6)$$

where U_o is the energy absorbed/unit volume. Note that U_o depends only on the longitudinal properties $(\sigma_x)_{max}$ and E_x. From Eqs. (5) and (6) it can be seen that U_o is independent of s/d beyond the critical value of s/d and depends only on the ultimate tensile (bending) strength and modulus. For values of s/d less than the critical value, the energy absorbed/volume decreases as the maximum value of σ_x decreases with s/d. The material thus has a lower energy absorbing capability when the failure is in shear than when it fails in tension. The value of E_o also decreases with s/d. These observations are all based on the assumption of linear elastic behavior to failure.

2.2 DEFLECTION DUE TO SHEAR

Beams having a small length to depth ratio and beams of anisotropic materials having shear moduli much smaller than their tensile moduli have shear stresses which can cause significant in-plane shear deformation and

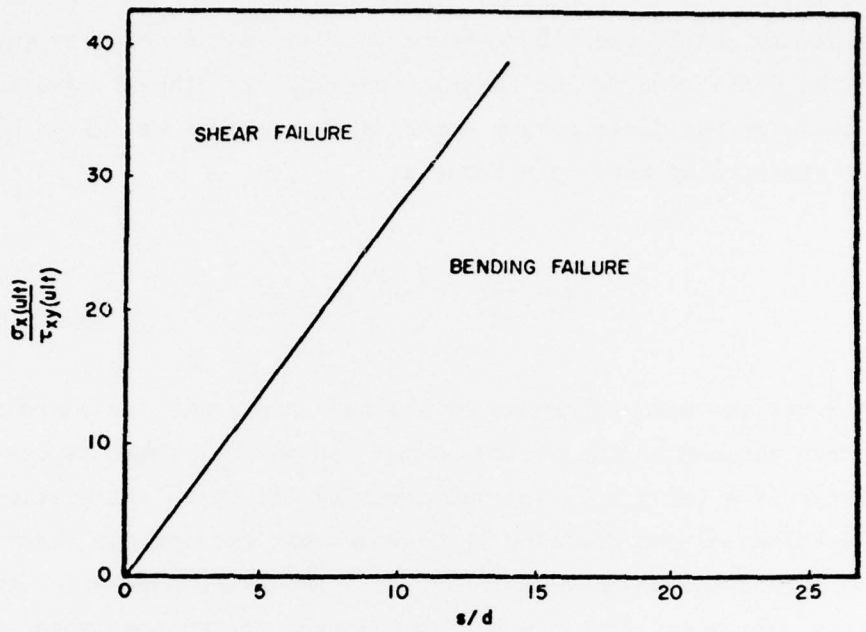

Figure 2. Failure regimes.

possibly even shear yielding. This deformation produces additional deflection which may have to be considered.

Deflection due to elastic shear deformation in an isotropic elastic material can be calculated using the theory of elasticity. A deflection equation for rectangular beams including shear deformation effects is presented in Reference 2 as;

$$\delta = \frac{Ps^3}{48EI}\left[\ 1 + 1.096\ (\frac{d}{s})^2\ \frac{E}{G}\right]\ . \qquad (7)$$

The term outside the brackets is the elementary beam formula, the term on the right in brackets represents the correction due to elastic shear deformation. Deflection due to shear is thus significant for small values of s/d or large values of E/G.

If the shear stresses in bending exceed the shear yield stress of the material, additional deflection due to shear yielding will occur. To calculate the deflection caused by shear deformation (including shear yielding), a model was developed which assumes a bilinear shear stress-strain curve for the material. The elastic and plastic moduli in shear were denoted by G and

G_p, respectively, while the yield stress in shear was denoted by τ_y. To calculate the deflection due to shear, including yielding, it was assumed that the shear stress distribution across the thickness was given by the elementary strength of materials formula;

$$\tau = \frac{3P}{wd^3}(c^2-y^2), \tag{8}$$

where $c = \frac{d}{2}$ was the half thickness of the beam and y was the coordinate measured from the centerline of the beam. The maximum shear stress occurs at the center (i.e. at y = 0) and was given by Eq. (2). Integrating Eq. (8) across the thickness and dividing by d shows that the average shear stress equals two-thirds the maximum shear stress. From this parabolic stress distribution, the shear strain was obtained from the assumed shear stress-strain curve (i.e. an elastic linear strain hardening model). The plastic shear strains were assumed not to influence the shear stress distribution for the purpose of computational simplicity. The half-depth of the yield region as measured from the centerline of the beam was;

$$y_{yield} = c\alpha^{1/2}, \tag{9}$$

where;

$$\begin{aligned} \alpha &= 1 - \frac{\tau_{yield}}{\tau_{max}} && \tau_{max} > \tau_{yield} \\ &= 0 && \tau_{max} < \tau_{yield} \end{aligned} \tag{10}$$

The shear strains were calculated from the stress-strain curve and then integrated across the thickness to obtain an average shear strain at each cross-section. This average shear strain was then used to calculate the mid-span deflection of the beam due to shear as;

$$\delta = \frac{\tau_{max}s}{3G}\left[1 + \alpha^{3/2}\left(\frac{G}{G_p} - 1\right)\right] \tag{11}$$

where G_p was the plastic modulus in shear and α was defined in Eq. (10). The term outside brackets represents the elastic deflection due to shear. The term on the right side of the brackets represents the additional contribution due to shear yielding within the yield region defined by Eq. (9).

2.3 STRESSES AND DEFLECTIONS UNDER LOADING TUP

It is apparent that the stress state near the loading tup of a beam differs from that calculated using simple strength of materials principles in which local compression in the thickness direction is not considered. For small loads where yield stresses are not exceeded, the beams can be treated as linear orthotropic materials. Contact stress solutions exist for orthotropic materials (see Reference 3), but solutions for isotropic elastic materials are less complicated and are used here for a first approximation.

If one assumes isotropic elastic material behavior and no contact friction then the loading distribution is elliptical over a width 2b and is specified as follows (Reference 4);

$$\sigma_{max} = \frac{2}{\pi} \frac{P}{wb} , \tag{9a}$$

where;

$$b = \frac{2}{\pi} \frac{P}{w} \Delta , \tag{9b}$$

and;

$$\Delta = \frac{2}{\frac{1}{R_T} + \frac{1}{R_B}} \frac{1-\nu_T^2}{E_T} + \frac{1-\nu_T^2}{E_B} . \tag{9c}$$

Subscripts T and B refer to the loading tup and beam, respectively; ν is Poissons ratio, and R is the radius of curvature.

With the contact pressure known, the beam stress state can be calculated from theory of elasticity formulas.

Consider a simply supported beam with cosinusoid loading such that the beam end has a loading node and the net force is resisted by shear forces

on the ends. The resulting stress state, presented in Reference 5, is given by;

$$\sigma_x(x,y) = \left[A \cos \alpha x \, \frac{(\alpha c \cosh \alpha c - \sinh \alpha c) \cosh \alpha y - \alpha y \sinh \alpha y \sinh \alpha c}{\sinh 2\alpha c + 2\alpha c} \right.$$

$$\left. - \frac{\alpha c \sinh \alpha c - \cosh \alpha c) \sinh \alpha y - \alpha y \cosh \alpha y \cosh \alpha c}{\sinh 2\alpha c - 2\alpha c} \right] , \qquad (11a)$$

$$\sigma_y(x,y) = A \cos x \left[\frac{(\alpha c \cosh \alpha c + \sinh \alpha c) \cosh \alpha y - \alpha y \sinh \alpha y \sinh \alpha c}{\sinh 2\alpha c + 2\alpha c} \right.$$

$$\left. \frac{(\alpha c \sinh \alpha c + \cosh \alpha c) \sinh \alpha y - \alpha y \cosh \alpha y \cosh \alpha c}{\sinh 2\alpha c - 2\alpha c} \right] , \qquad (11b)$$

$$\tau_{xy}(x,y) = A \sin x \left[\frac{\alpha c \cosh \alpha c \sinh \alpha y - \alpha y \cosh \alpha y \sinh \alpha c}{\sinh 2\alpha c + 2\alpha c} \right.$$

$$\left. \frac{\alpha c \sinh \alpha c \cosh \alpha y - \alpha y \sinh \alpha y \cosh \alpha c}{\sinh 2\alpha c - 2\alpha c} \right] , \qquad (11c)$$

where;

$$\alpha = \alpha_n = (2n-1) \frac{\pi}{s} , \; 1,2,3..... \quad . \qquad (11d)$$

The actual elliptical loading distribution at the mid-span can be approximated by a fourier series of these cosinusoids. The resulting stress state is calculated as the summation of the stress states due to each of the terms of the fourier representation of the actual load.

The local indentation of the beam, due to the loading tup, particularly in thick beams where loads are greater, increases the magnitude of the measured deflection. This indentation can be calculated from a knowledge of the contact stress distribution and the stress state in the vicinity of the load in addition to the material constitutive equations for these anisotropic materials. Because of the complexity of such a calculation, it was decided instead to calculate an upper bound for the indentation based on a very simple model. Assume the loading distribution to be elliptical and

consider the region under the loading tup to be composed of thin, independent, vertical slices. Each of these slices is compressed by the load above it in proportion to the loading, hence, the indented shape is also elliptical. The maximum depth of indentation is

$$\delta_{in} = \frac{(\sigma_y)_{max}}{E_y} d \ , \tag{12}$$

where E_y is the modulus in the y direction and it is assumed that the stresses, σ_y, are uniform through the thickness. In reality the slices are not independent, indeed, the actual deformed shape includes more than the contact area. It is also known that the stresses are not uniform through the thickness but must approach zero at the lower surface. If it is assumed that the contact stresses do not exceed the yield strength of the material, then the maximum indentation is less than the calculated value from Eq. (12).

SECTION III
EXPERIMENTAL PROCEDURE

A series of three point bend tests were conducted over a range of rates. The procedures used to obtain data from these tests are described in this section.

3.1 MATERIAL AND SPECIMENS

Three unidirectional fiber composite materials were tested; graphite-epoxy T-300, SP-313 (Gr/Ep); 8 mil boron-1100-F-aluminum (B/Al-1100) and 5.6 mil boron-6061-F-aluminum (B/Al-6061. All had 50 percent fibers by volume. The boron-aluminum materials were obtained from United Technologies Research Center while the graphite-epoxy specimens were fabricated at the Air Force Materials Laboratory (AFML). The B/Al-6061 had a uniaxial tensile strength of 2.07 GN/m^2 (300 ksi) which is relatively strong for this material; the B/Al-1100 had a tensile strength of 1.31 GN/m^2 (190 ksi) which is unusually low. The boron-aluminum specimens were tested with the axis of the beam in both longitudinal fiber and transverse fiber directions; the graphite-epoxy specimens were all tested in the longitudinal direction. Tests were conducted at three different loading rates using three different apparatus described below. Four thicknesses were used for the boron-aluminum tests and three for the graphite-epoxy. The test matrix, indicating the number of specimens tested in each condition, is presented in Table 1. All specimens were unnotched.

3.2 TEST PROCEDURE

Slow bend tests were conducted using a test fixture machined to the standard Charpy geometry and capable of being mounted in both Instron and MTS hydraulic testing machines. A 1.25 cm (0.5 in) LVDT was used to measure head to head displacement while load was measured by a standard compressive load cell. Load versus displacement was recorded on a Hewlett-Packard X-Y plotter. The LVDT was calibrated with the aid of a dial gauge; load

was calibrated with calibrations weights. A crosshead rate of 0.0004 cm/s (0.0002 in/s) was used in all the slow bend tests.

TABLE 1. SPECIMEN TEST MATRIX

	(in) d (cm)	Slow Bend	Intermediate	Charpy (Dynatup)
Gr/Ep	0.100 0 .25	8	-	1
	0.200 0 .51	8	-	1
	0.340 0 .86	8	-	1
B/Al-1100(L)*	0.100 0 .25	1	1	1
	0.150 0 .38	1	1	1
	0.200 0 .51	1	1	1
	0.250 0 .64	1	1	1
B/Al-1100(T)*	0.100 0 .25	1	1	1
	0.150 0 .38	1	1	1
	0.200 0 .51	1	1	1
	0.250 0 .64	1	1	1
B/Al-6061(L)	0.100 0 .25	1	1	1
	0.150 0 .38	1	1	1
	0.200 0 .51	1	1	1
	0.250 0 .64	1	1	1
B/Al-6061(T)	0.100 0 .25	1	1	1
	0.150 0 .38	1	1	1
	0.200 0 .51	1	1	1
	0.250 0 .64	1	1	1

*L - Longitudinal Fiber Direction
T - Transverse Fiber Direction

Several photographs were taken of the graphite-epoxy specimens in an effort to define the delamination progression using a camera supported directly in front of the specimen. The manually operated camera was triggered after audible failures.

Intermediate rate tests were conducted using the same test fixture as in the slow bend tests. The fixture was mounted in a 22 kN (5000 lb) machine which is capable of achieving crosshead velocities in excess of 50 cm/s (20 in/s). The intermediate rate tests were all conducted at a crosshead rate of 2.5 cm/s (1.0 in/s) which is well within the machine capability for achieving accurate stroke control. Deflection and force were measured as in the slow bend test and recorded on an x-y oscilloscope with the aid of a Polaroid camera.

High-rate, instrumented Charpy impact tests were conducted on a 217-J (160 ft-lb) Tinius Olsen pendulum impact machine instrumented with a Dynatup loading tup and associated electronics from Effects Technology, Inc. Load calibration had previously been performed using standard notched specimens of a rate insensitive aluminum alloy. The pendulum provided an impact velocity of 250 cm/s (100 in/s) which was verified to be accurate to better than two percent. This velocity corresponded to 85 J (62.9 ft-lb) of input energy. In the tests, most specimens absorbed only 1.4 to 2.7-J (1 to 2 ft-lb) of energy although one absorbed 27 J (20 ft-lb). The load versus time curves were recorded on a storage oscilloscope and photographed. A 5.1 kHz filter in the Dynatup instrumentation was used to filter out high frequency noise and oscillations in the loading tup.

3.3 DATA REDUCTION

The data from the slow and intermediate rate tests, consisting of chart and oscilloscope records of load versus deflection, was digitized using an electromagnetic digitizer with 0.027 cm (0.01 in) resolution. A Hewlett-Packard Model 9820A calculator was used to reduce the digitized data which was then plotted as normalized load against deflection curves. The load versus time data from the Dynatup was numerically integrated using the continuously corrected velocity of the pendulum to calculate deflection. The energy absorbed by the specimen equals the kinetic energy lost by the pendulum in the calculation of pendulum velocity.

In all tests, specimen dimensions were measured prior to testing. Small variations from the nominal dimensions were found for each geometry. In order to correct for these small variations in dimensions, the load-deflection curves were normalized to the nominal values for each of the thicknesses

tested. The load was multiplied by $\frac{w_{actual}}{w_{nominal}} \left(\frac{d_{actual}}{d_{nominal}}\right)^2$. The deflection was multiplied by $\frac{w_{nominal}}{w_{actual}} \frac{d_{nominal}}{d_{actual}}$. All load-deflection curves were reduced to this normalized form for comparison purposes.

SECTION IV
RESULTS AND DISCUSSION

The results collected from the experiments consisted of load-deflection records and energy absorption measurements. These are discussed in detail in this section.

4.1 LOAD-DEFLECTION RELATIONS

The strength of materials load-deflection formula for slender beams, together with the value of the elastic modulus determined from tensile data, can be used to predict the beam load-deflection relationship assuming linear elastic behavior. Figures 3, 4, and 5 present the experimental results for the thinnest (0.25 cm) beams for each of the three materials together with the theoretical prediction assuming failure at the maximum experimentally observed load. The graphite-epoxy and boron/aluminum-6061 are essentially linear in response, but the initial compliance is actually greater (lower modulus) than predicted. This implies that phenomena other than pure bending are contributing to the deflection, even at stress levels well below failure. Figure 3 shows that the 1100 boron-aluminum is not as well predicted in that the actual behavior is non-linear in addition to displaying a higher initial compliance.

For all of the beams of various thicknesses the actual initial compliance was greater than the theoretical prediction. The elastic modulus (E_x) in bending was computed from the initial slopes and is plotted versus slenderness in Figure 6. For each material, it is seen that the observed modulus approaches the tensile modulus as the slenderness ratio s/d increases. Thus, in order to measure the modulus from a bend test, a high slenderness ratio is required. As thickness increases, other phenomena contribute to the beam deflection. Even for the thinnest beam tested, corresponding to s/d of approximately 16, the tensile modulus was not well predicted as shown in Figure 6.

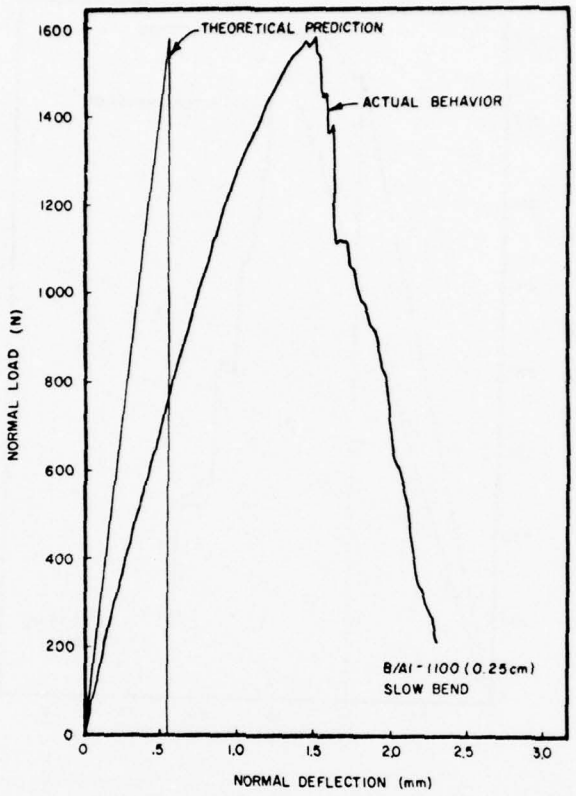

Figure 3. Load versus deflection, slow bend (B/Al-1100, 0.25 cm thick).

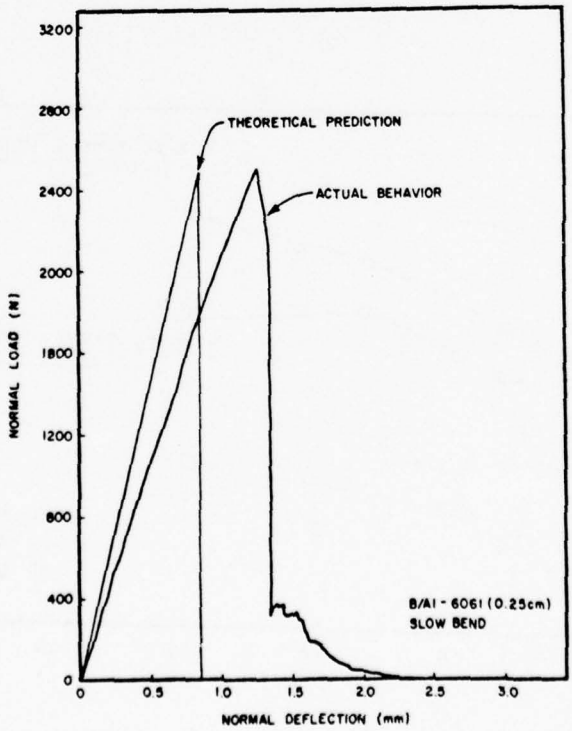

Figure 4. Load versus deflection, slow bend (B/Al-6061, 0.25 cm thick).

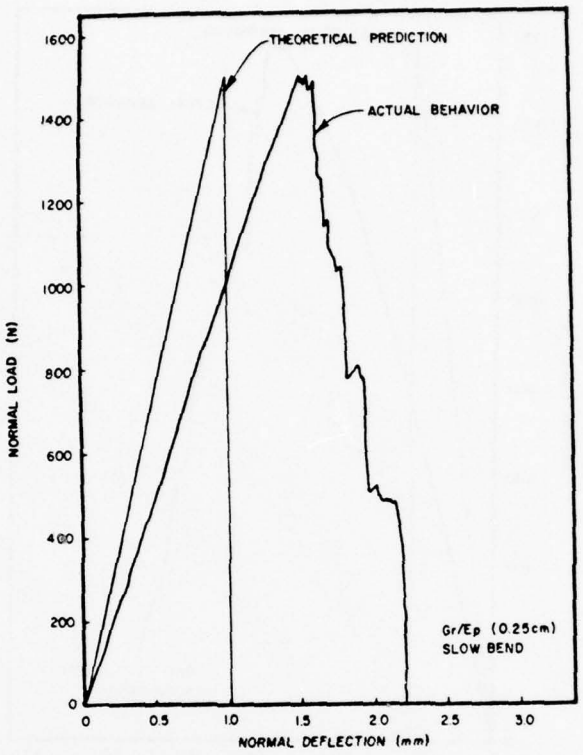

Figure 5. Load versus deflection, slow bend (Gr/Ep, 0.25 cm thick).

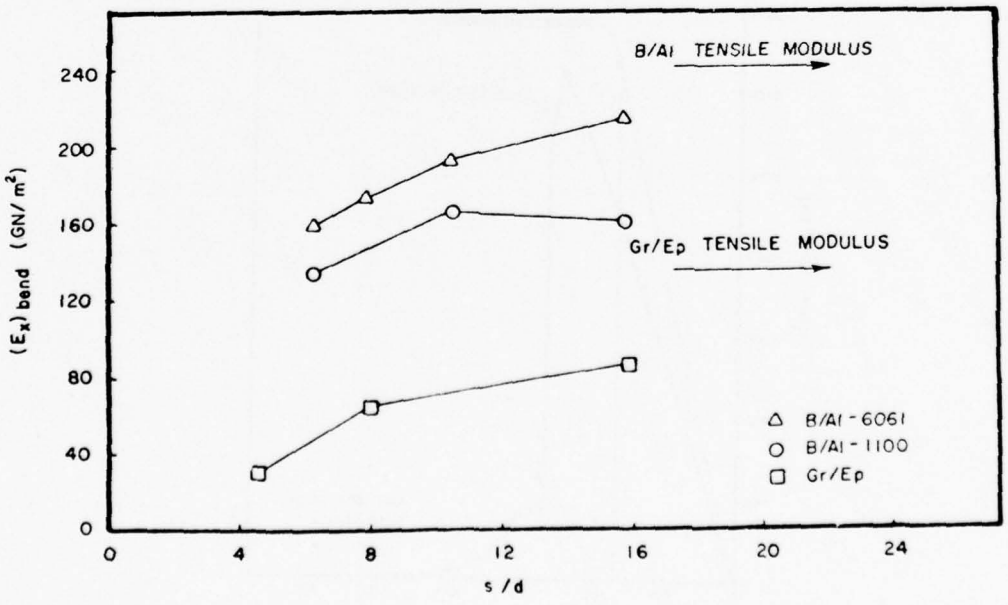

Figure 6. Bending modulus versus slenderness ratio (slow bend data).

To explain the discrepancy in observed versus predicted modulus, other effects which might contribute to deflection were considered. Table 2 presents the additional compliance due to elastic shear deformation and indentation as calculated from Eqs. (7) and (12). The data are presented in the form of calculated and observed values of beam compliance. The data show that the deflection due to elastic shear deformation is small in comparison to bending with the exception of the thick graphite-epoxy beam. The value shown for indentation is an upperbound as given by Eq. (12) based on several conservative assumptions; the actual indentation is probably much less. The calculated indentation values were larger for the thick beams because of the higher loads involved. With both of these corrections, the actual initial compliance of the beams was still greater than that predicted analytically.

		Compliance (mm/MN)				
Material	d (cm)	Bending	Elastic Shear Deformation	Indentation	Predicted Total	Measured Total
Graphite Epoxy	0.25	708	78	51	788-839	1091
	0.51	89	39	56	128-184	194
Boron-Aluminum-1100	0.25	393	8	9	401-410	640
	0.38	116	5	9	122-131	166
	0.51	49	4	10	53-63	86
	0.64	25	3	12	29-40	44
Boron-Aluminum-6061	0.25	393	8	7	401-408	491
	0.38	116	5	7	122-128	131
	0.51	49	4	8	53-61	74
	0.64	25	3	8	29-37	38

To further improve the analytical predictions of deflection, the yielding of the beams in shear was also considered. It was noted that the thin B/Al-6061 and Gr/Ep beams showed nearly linear load-deflection curves (see Figures 4 and 5). This suggests that the longitudinal properties are nearly linear elastic to failure

for these two materials, an observation which can be confirmed from tensile tests. However, Figures 7 and 8 show that the load-deflection curves of the thickest beams tested are quite nonlinear. The prefailure shape shows that some yielding occurs. Since the stress state of thick beams differs from that in thin beams in that higher shear stresses occur, the data suggest that the yielding which occurs is due to shear.

Figure 9 compares the results of the shear yielding model developed above with the experimental data for 6061 boron-aluminum. The model, as outlined above, is based on an elastic-plastic with strain hardening shear stress-strain relationship. The values of shear yield stress and plastic modulus were not known, but were chosen to achieve good correlation with the experimental data. Values of 63 MN/m^2 (9.2 ksi) and 1.5 MN/m^2 (220 ksi) were chosen for yield stress and plastic modulus, respectively. This model displays the proper behavior (i.e. increased compliance due to shear yielding). The experimental data shows that the beam appears to yield more gradually, suggesting that the actual beams have either a slower growth of the plastic region, perhaps related to contact induced stresses, or a non-linear shear stress-strain behavior as opposed to the assumed bilinear model. The effect of shear yielding on energy absorption will be discussed later.

4.2 CONTACT STRESS STATE AT FAILURE

The failed specimens and the photographs taken during the testing were examined to determine the location of the first failure for the thicker graphite-epoxy beams. Each of these failures initiated near the mid-span plane and propagated to the nearest end. Most of the specimens did not fail at the mid-depth plane as a strength of materials analysis predicts but nearer the loading point. This suggests that the contact induced stress state resulted in the location of maximum shear stress being nearer the loading point.

Figures 10 and 11 compare contact induced stress state calculated with the theory of elasticity (Eq. (11), with the strength of materials prediction. The beam geometry and properties were chosen to be those of the thick graphite-epoxy beam. Figure 10 shows that the two solutions for longitudinal stresses are nearly identical at a section away from the loading, but the contact induced stresses cause higher longitudinal compressive stress in a

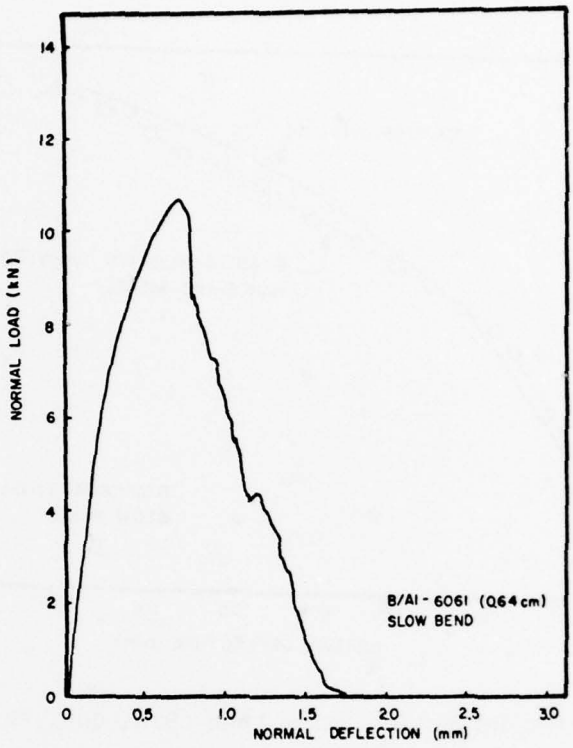

Figure 7. Load versus deflection, slow bend (B/Al-6061, 0.64 cm thick).

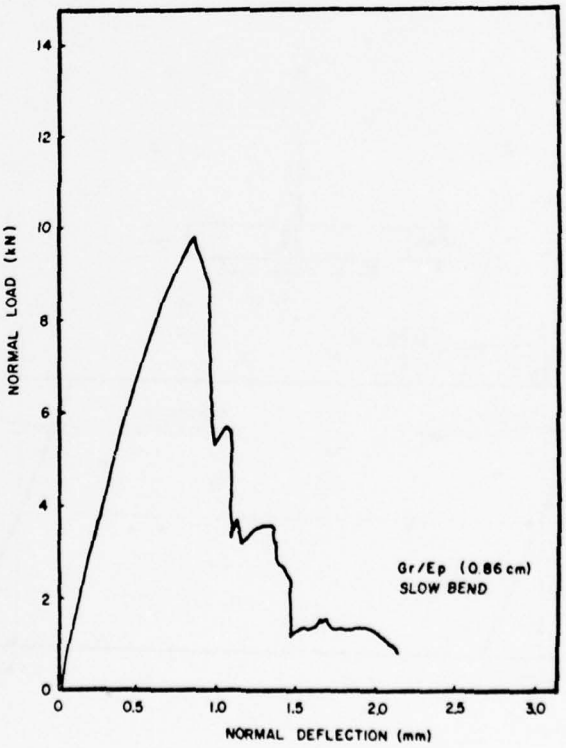

Figure 8. Load versus deflection, slow bend (Gr/Ep, 0.86 cm thick).

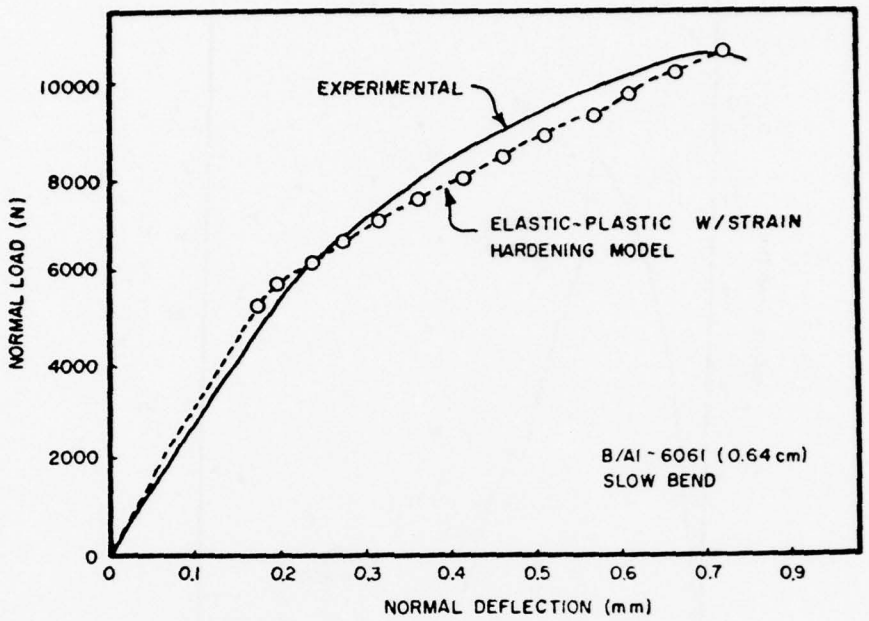

Figure 9. Load versus deflection, slow bend (B/Al-6061, 0.64 cm thick).

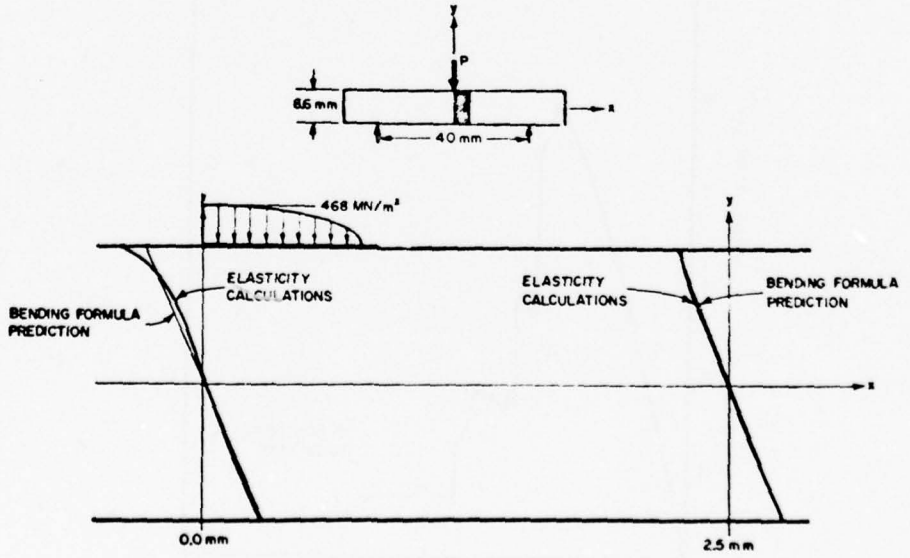

Figure 10. Elastic longitudinal stress distribution in graphite-epoxy.

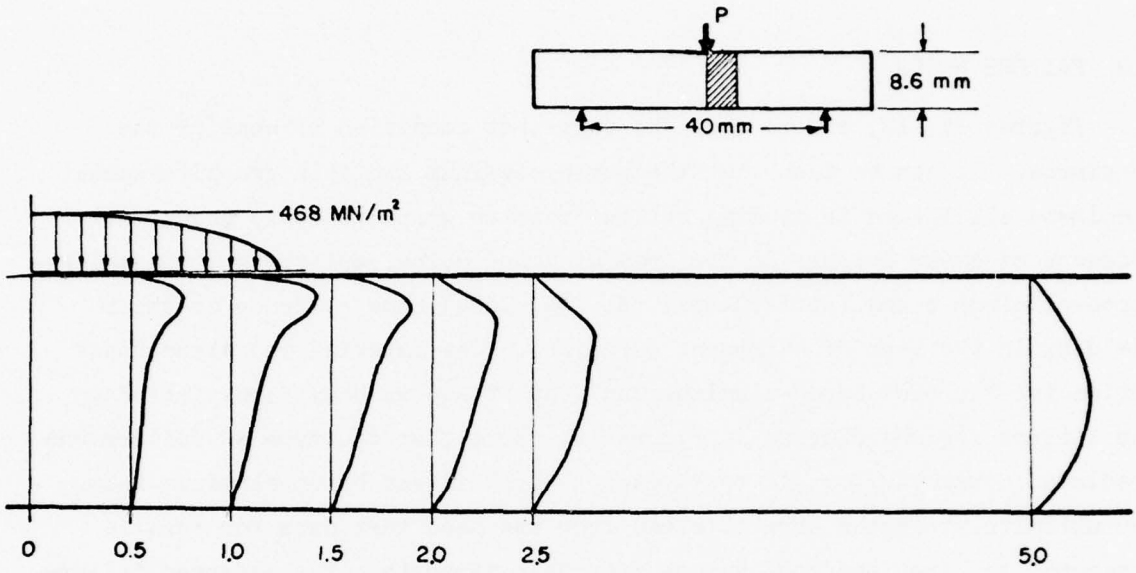

Figure 11. Elastic shear stress distribution in graphite-epoxy (including contact stresses).

small region near the loading area. In Figure 11 note that the shear stress distribution at a section away from the loading is nearly parabolic and nearly equal in magnitude to the strength of materials prediction, but in a small region about the loading area, the location of maximum shear stress approaches the loading point and the magnitude of the maximum shear is greater than strength of materials predicts. Thus, the elasticity solution shows the proper trend compared to the strength of materials prediction. However, the difference turns out to be too extreme. The location of maximum shear stress is too shallow and the magnitude too great for the material to have not failed earlier. It may be that this model would be more accurate except that shear yielding relaxes the contact induced stress and resulting increased local curvature increases the contact area and lowers the stresses. Shear yielding in a region growing from the contact point could probably explain the more gradual yielding observed in the experimental data (see Figure 9). It was concluded that the actual stress state is bounded by the elasticity and the strength of materials solutions.

4.3 FAILURE MODES

Figures 12, 13, and 14 show the post-test condition of some of the specimens. It can be seen that the boron-aluminum and thin graphite-epoxy specimens all failed in bending but the thicker graphite-epoxy beams show evidence of shear failure in the form of longitudinal splitting. The thick boron-aluminum beams (particularly the B/Al-1100) show evidence of shear yielding in the form of permanent curvature. The material and slenderness ratios for the 6061 boron-aluminum and graphite-epoxy beams are plotted on the failure regimes diagram in Figure 15. Note that the type of failure was predicted correctly for all tests except the thickest boron-aluminum beam. The ultimate strengths were obtained from the bend test data for tensile strengths and from handbook values for shear strength. The observed failure of the thick boron-aluminum beam would appear to indicate that either the ultimate shear strength was higher or, more likely, the assumptions of linear elastic behavior and the strength of materials formulas for calculating stress were not valid. In particular, the effects of shear yielding were probably important. Because of the large amount of shear yielding and the non-linear behavior of the B/Al-1100, these data were not plotted on the failure diagrams.

Figures 16, 17, and 18 show the relationship between strength and slenderness ratio using the interaction chart (see Figure 1) to plot the experimentally observed strengths. Note, that the slender beams have tensile strengths in bending which are higher than the uniaxial tensile strength, an effect which is commonly explained by statistics and size effects. (The highly stressed volume of the beam is much smaller than that of a tensile specimen, hence, there is a statistically lower chance of a weak region failing first or of a flaw propagating to failure.) The thick beams, however, appear weaker than a tensile specimen. Since even these thick beams have smaller highly stressed volumes than that of a tensile specimen, size effect does not explain this phenomenon. These low strength bending failures occur in specimens with slenderness ratios near those which lead to shear failure first. It thus appears that these apparently premature failures are shear stress influenced.

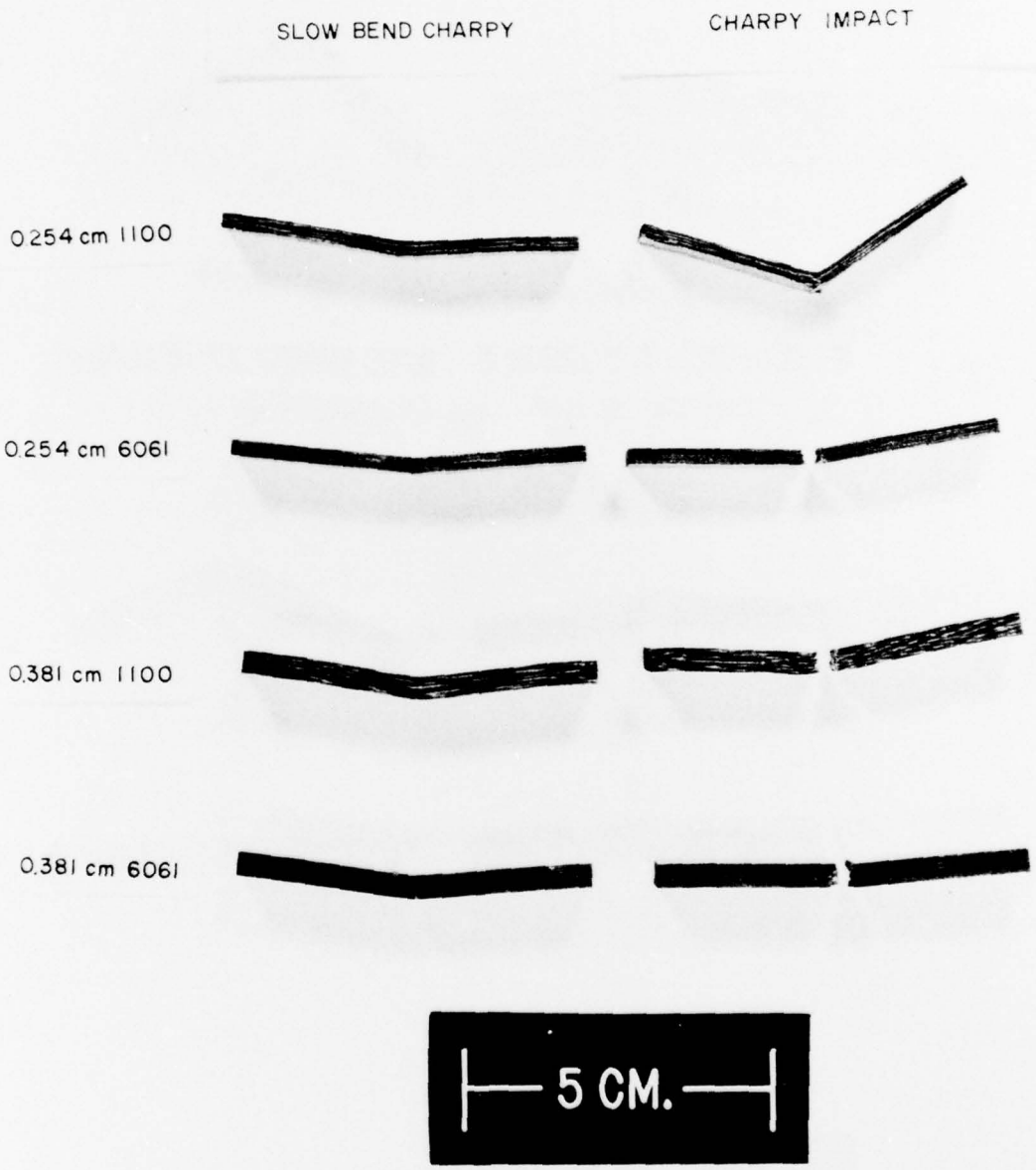

Figure 12. Post-test boron-aluminum specimens.

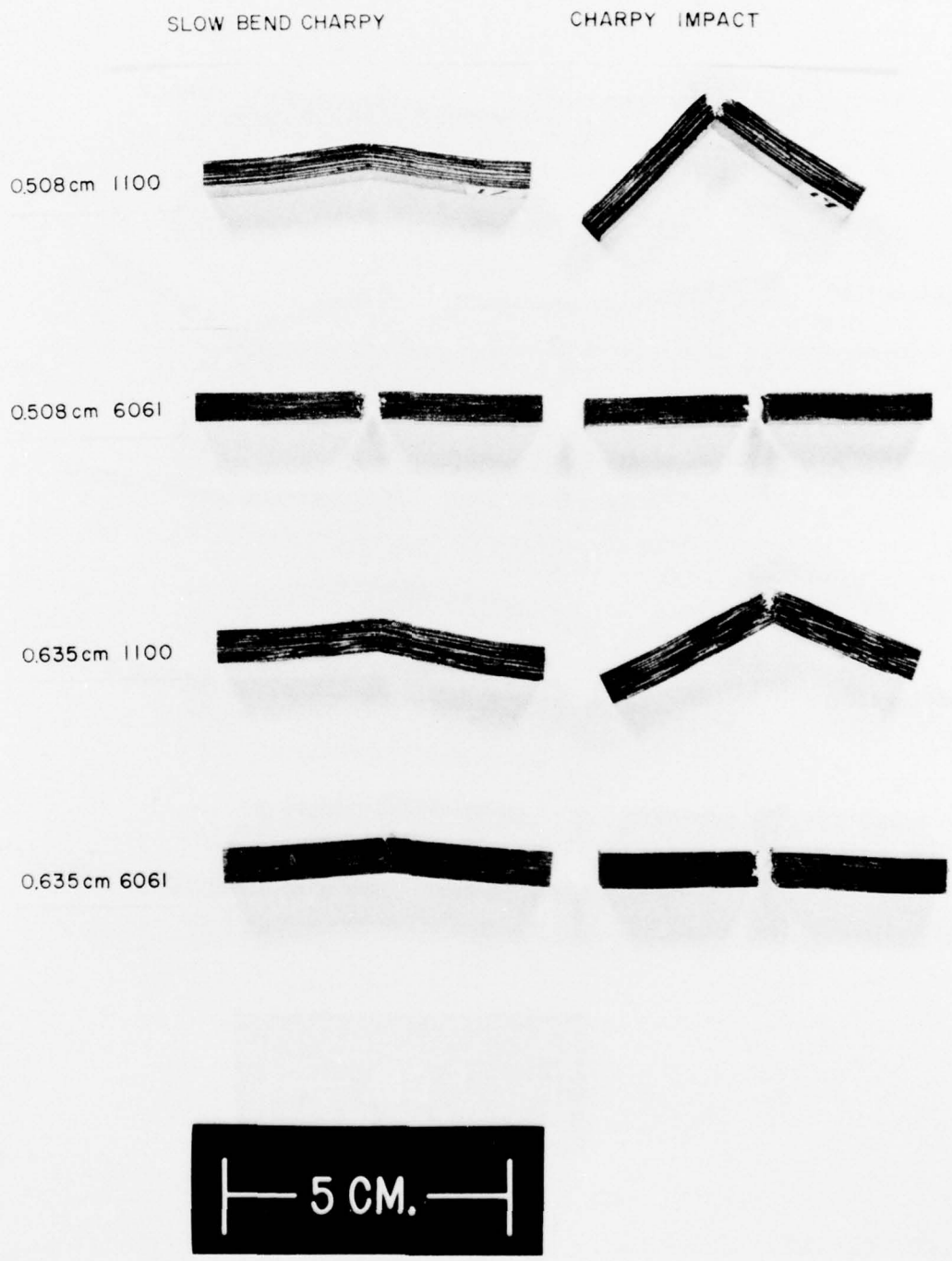

Figure 13. Post-test boron-aluminum specimens.

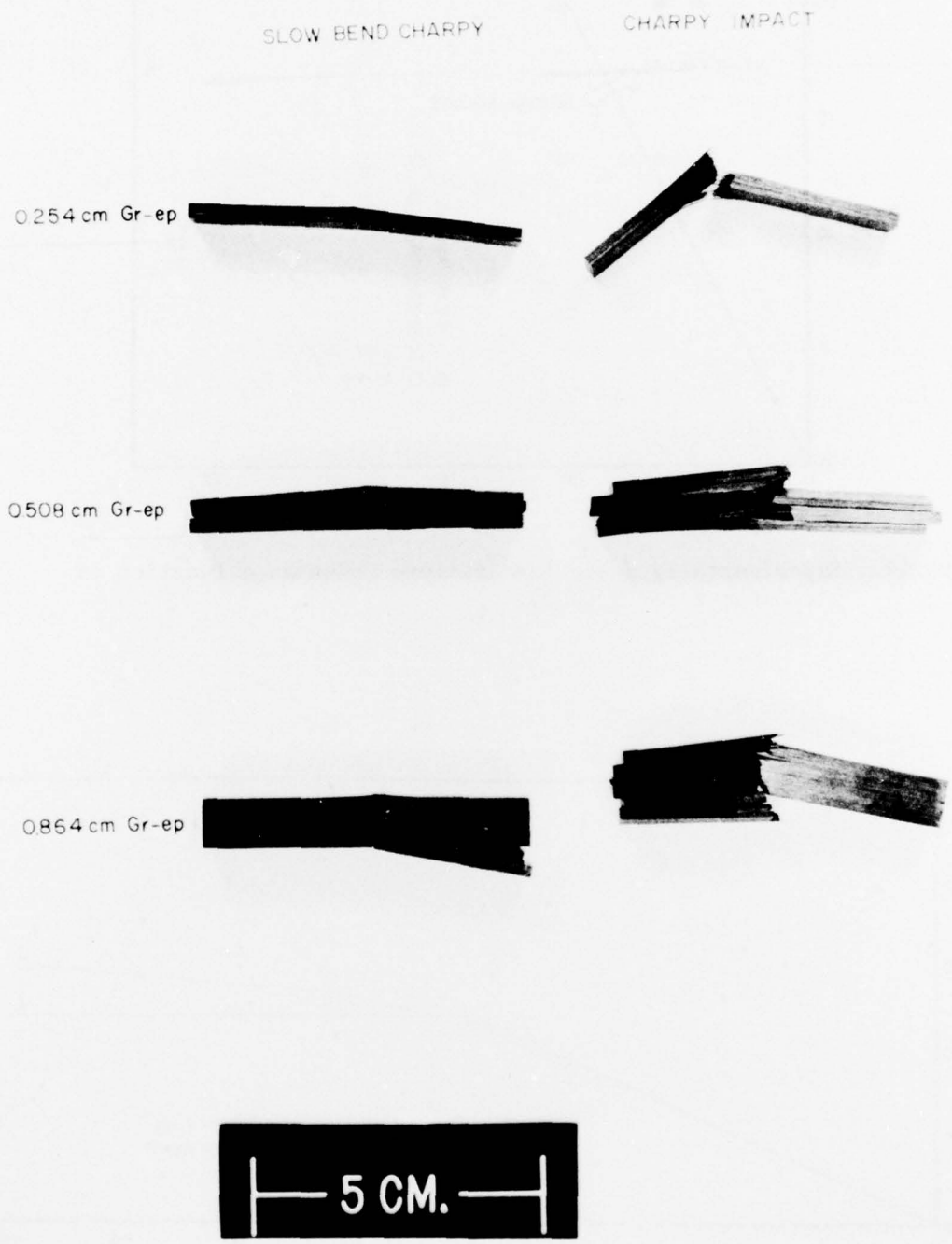

Figure 14. Post-test graphite-epoxy specimens.

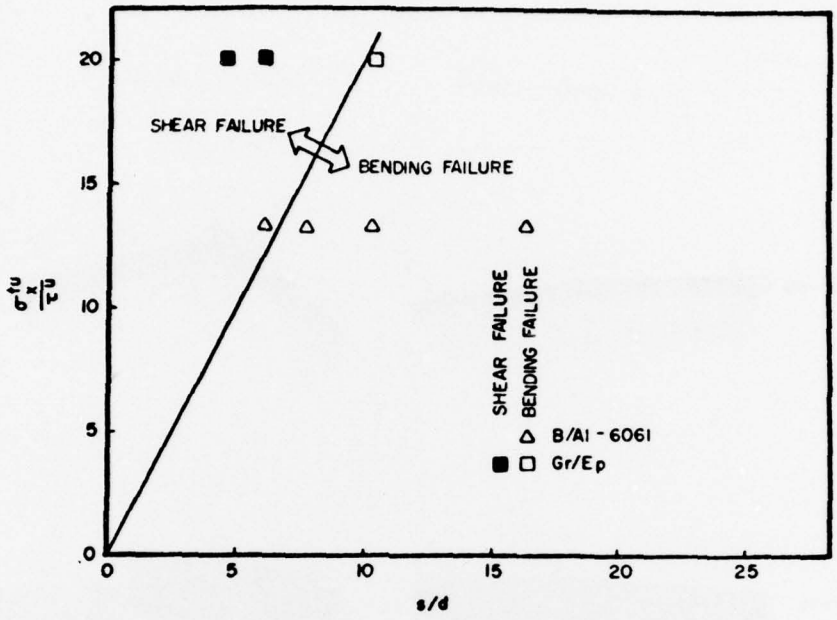

Figure 15. Experimentally determined failure modes as a function of slenderness ratio (s/d).

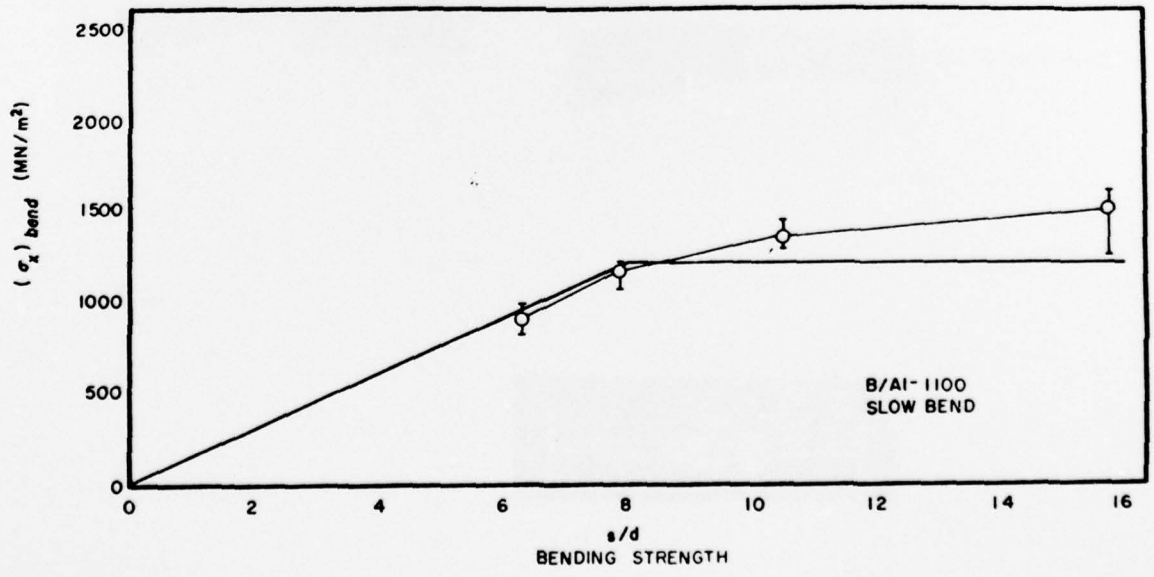

Figure 16. Flexural interaction diagram for B/Al-1100.

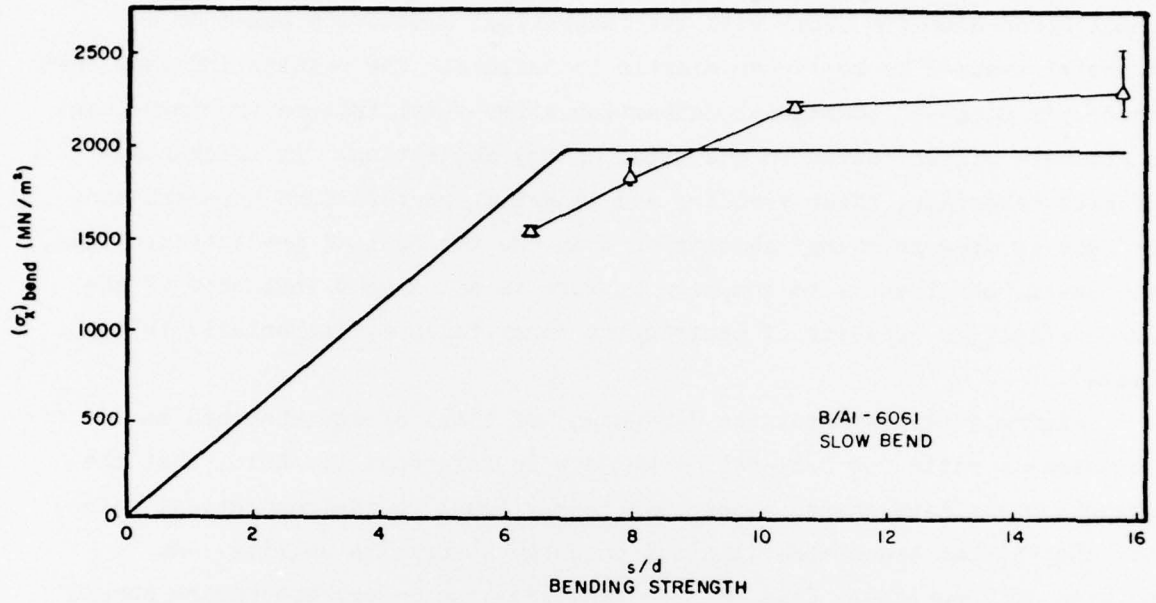

Figure 17. Flexural interaction diagram for B/Al-6061

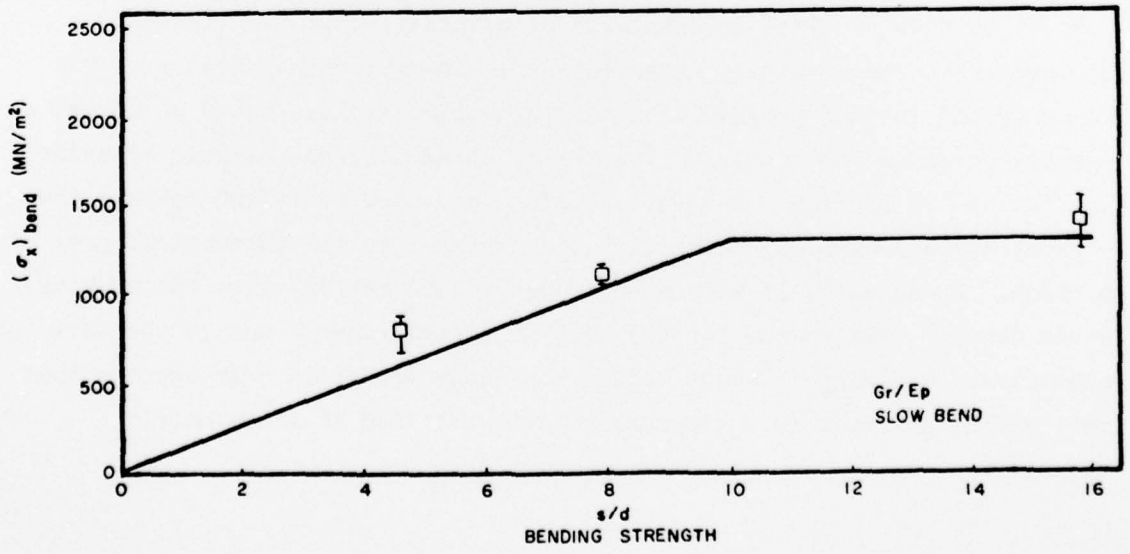

Figure 18. Flexural interaction diagram for Gr/Ep.

4.4 ENERGY ABSORPTION

Figures 19 and 20 compare the actual load-deflection curves of the thick boron-aluminum beams with the theoretical prediction based on a material assumed to be linear elastic to failure. The results indicate that shear yielding and additional deflection after first failure (maximum load) contribute significantly to the total energy absorption. In thick beams of both materials, shear yielding and lingering post-failure strength contribute to greater energy absorption than the theoretical prediction. Thus, the energy absorbed up to complete failure is not a good indicator of the load-deflection behavior of beams up to first failure, (especially thick beams).

Figure 21 illustrates the dependence of total energy absorbed on slenderness ratio for B/Al-6061 from data in Reference 1. Note, that the slender beams have energy absorption nearly equal to the theoretical value, but the thicker beams show increasing energy absorption ability. As pointed out previously (see Eqs. (5) and (6)) the energy absorption should decrease for s/d values less than the critical value where tensile and shear failure occur simultaneously. Although energy absorption for slender beams is dominated by tensile properties, for thicker beams it is influenced more by shear yield. It is proposed that if sufficiently slender beams are tested, their energy absorption and load deflection behavior will be closest to that predicted by strength of materials theory. Figure 22 compares the experimentally observed energy absorption capability of the beams tested in this program with the theoretical values based on ultimate tensile strength and modulus. The theory assumes linear elastic behavior and failure in bending. The experimental data show B/Al-1100 to have the highest energy absorbing capability, in contrast to the theoretical prediction. Presumably, if very slender beams were tested, then the ranking would change. The reason for the lack of correlation is due to the fact that significant yielding in shear occurs for these materials. It appears that this yielding effect is most pronounced in the 1100 aluminum matrix material.

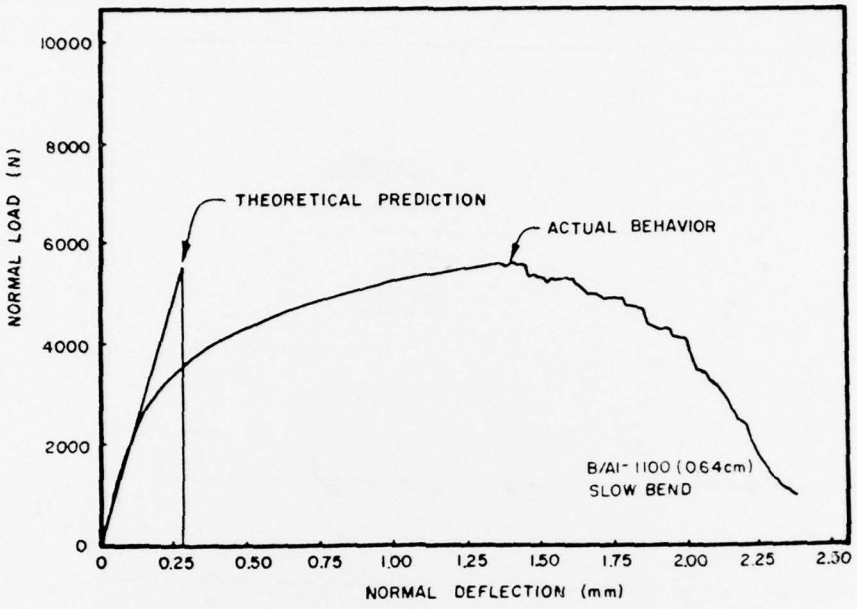

Figure 19. Load versus deflection, slow bend (B/Al-1100, 0.64 cm thick).

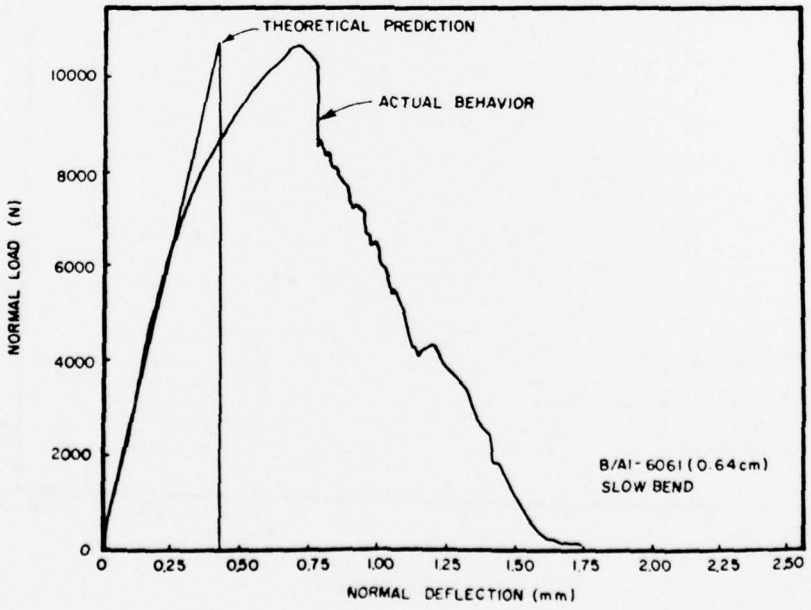

Figure 20. Load versus deflection, slow bend (B/Al-6061, 0.64 cm thick).

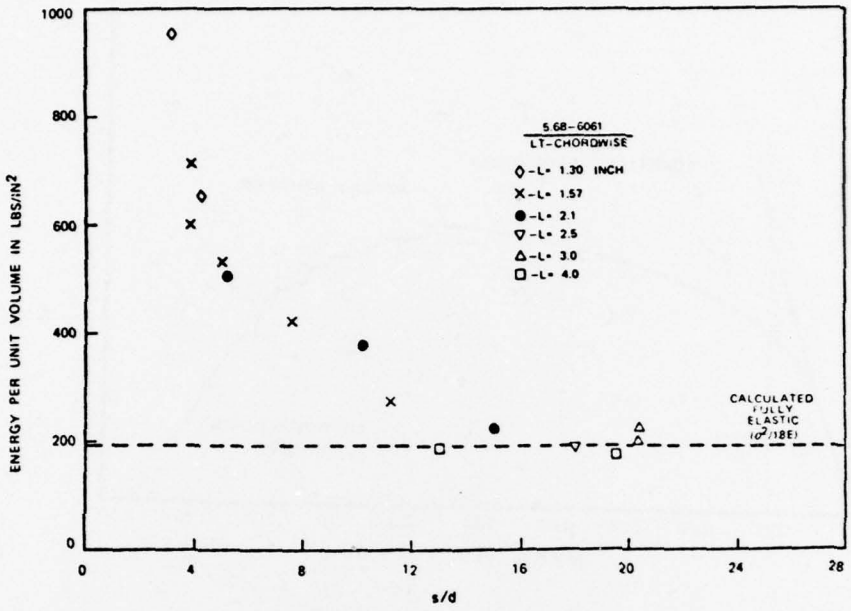

Figure 21. Energy per unit volume to maximum load (taken from Reference 1).

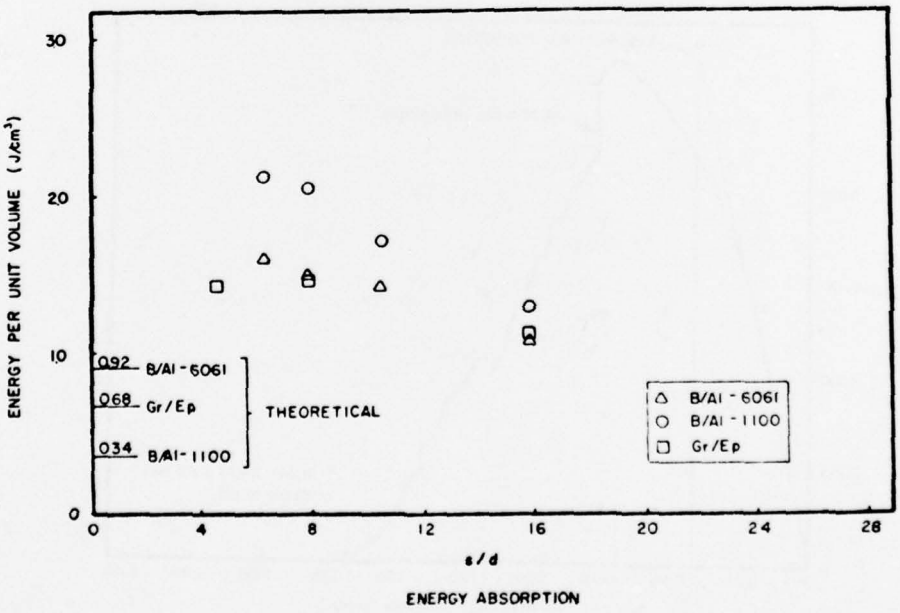

Figure 22. Energy absorption versus slenderness ratio.

4.5 OTHER EXPERIMENTALLY EXAMINED EFFECTS

4.5.1 Strain Rate Effects

The beams were tested at three different deflection rates to investigate rate effects, but since there was only one test of each material/depth/rate the data show much scatter. Figure 23 shows the effect of strain rate on bending strength for each of the test geometries and materials. A general trend of strength increasing with strain rate exists for most of the data but the magnitude of the rate effect appears small. Based on average values of rate sensitivity from tests of different thicknesses, the B/Al-6061 showed about one percent increase per decade in strain rate, the B/Al-1100 about two percent, and the graphite-epoxy three percent. Figure 24 shows the effect of strain rate on energy absorption for all of the tests. Again, a general upward trend exists, but there is too much scatter to draw any definitive conclusions.

4.5.2 Transverse Properties

The boron-aluminum beams were tested in both longitudinal fiber and transverse fiber orientations. Transverse strengths (matrix strengths) are shown in Table 3. The 6061 matrix was stronger and had less scatter than the 1100 material. Figure 25 shows typical transverse beam load-deflection relationships.

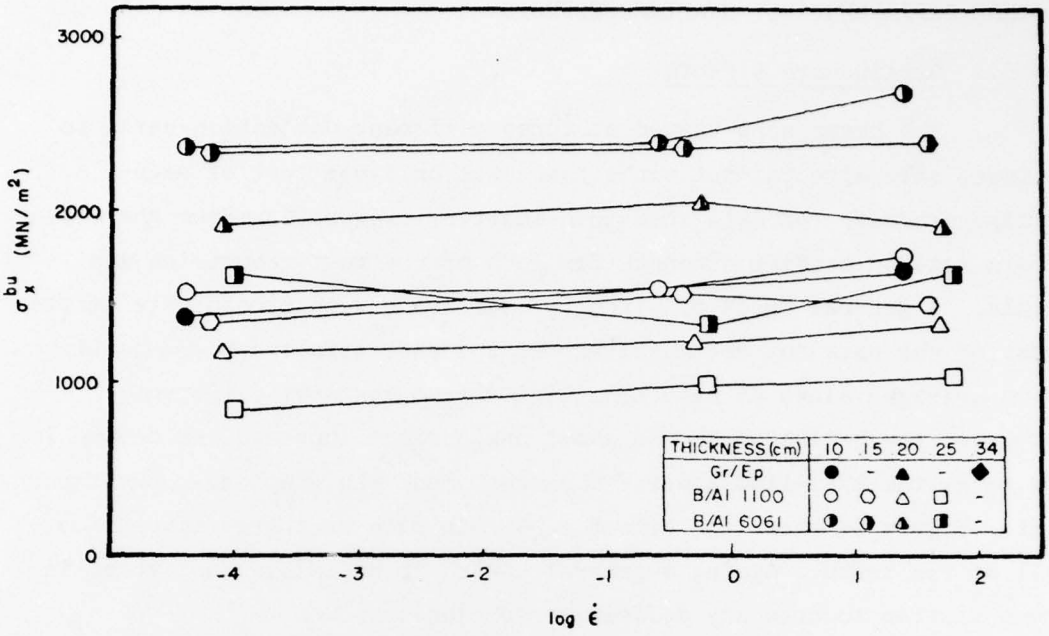

Figure 23. Effect of strain rate on ultimate bending strength.

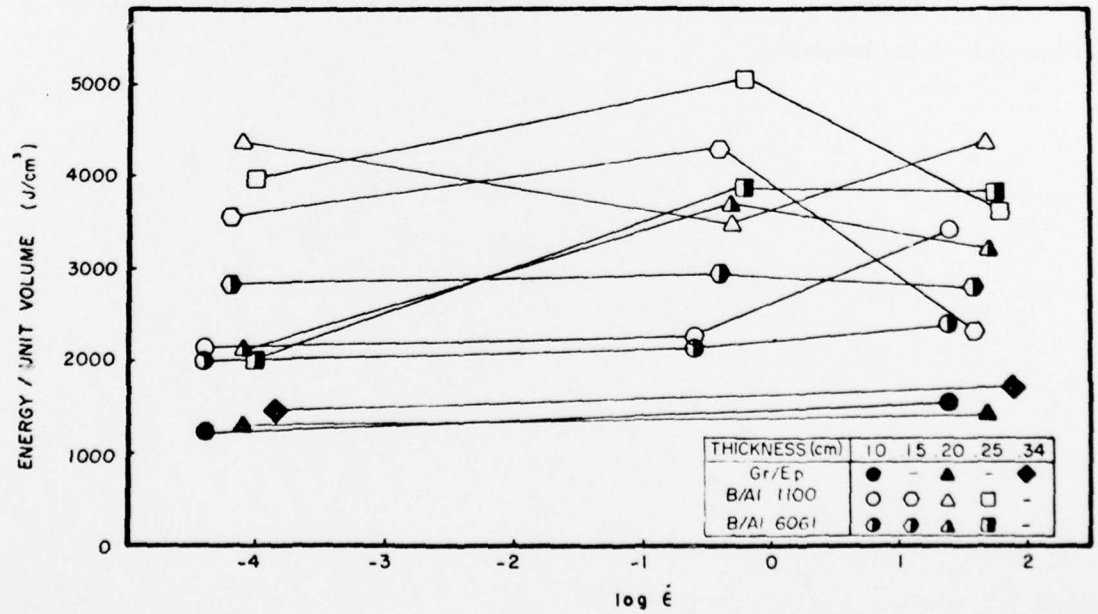

Figure 24. Effect of strain rate on energy absorption.

TABLE 3. SUMMARY OF TRANSVERSE PROPERTY FOR BORON-ALUMINUM

Material	Thickness d (cm)	Transverse Strength (MN/m^2) 0.0042 (mm/s) Load Rate	2.54 (mm/s) Load Rate	254 (mm/s) Load Rate	Average Value (MN/m^2)	Mean Deviation Deviation $\sigma/\bar{x}$
B/Al-1100	0.25	194	215	207	205	0.05
	0.38	200	207	224	210	0.06
	0.51	132	176	217	175	0.24
	0.64	95	126	140	121	0.19
Average (MN/m^2)		156	181	197	178	
Mean Dev.		0.33	0.22	0.22		0.24
B/Al-6061	0.25	380	389	351	373	0.05
	0.38	378	397	408	394	0.04
	0.51	367	377	387	377	0.03
	0.64	370	372	368	370	0.01
Average (MN/m^2)		374	384	378	379	
Mean Dev.		0.02	0.03	0.06		0.04

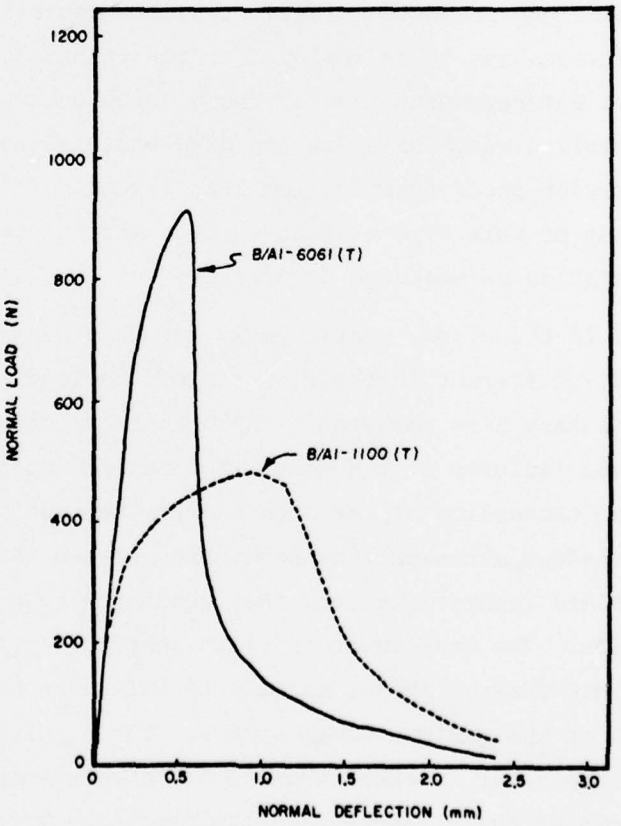

Figure 25. Load versus deflection for boron-aluminum specimens loaded transversely.

SECTION V
CONCLUSIONS

Three point bend tests on boron-aluminum and graphite-epoxy specimens of various thicknesses have shown that the behavior of composite materials in bending is difficult to predict and the interpretation of test results can be not only difficult, but sometimes misleading. Among the specific findings in this investigation were:

1. The deflection was greater in all cases than that predicted by either strength of materials formulas or more sophisticated analyses which also considered shear deform, shear yielding, and local indentation of the loading tup. Since the observed deflections or compliance was greater than predictions based on uniaxial tensile properties, either more sophisticated analyses have to be employed or the uniaxial properties (i.e. modulus) are not representative of those which occur in bending. The data are particularly disturbing since the discrepancies between observed and predicted behavior occur even for low load levels. It is recommended that future testing of this type utilize surface strain gauges and that loading tup indentation be measured accurately.

2. Stresses in the beams, particularly for the thicker ones, appear to be significantly different in the vicinity of the loading tup from those predicted by elementary beam formulas. These contact induced stresses influence the shear failures in the beam. The maximum shear stresses appear to occur above the centerline of the beam nearer the loading tup. The location of the maximum stresses lies somewhere between that predicted by strength of materials (centerline) and that predicted by a theory of elasticity solution. The non-linear or yield behavior of the material, particularly in interlaminar shear, appears to influence both the location and the magnitude of the maximum shear stress. Three point bend tests where first failures occur in shear thus do not appear to be a reliable method for determining the ultimate interlaminar shear strength of composite materials.

3. The energy absorbing capability of a beam in bending is highly dependent on the stress state in the beam which, in turn, depends on the geometry or slenderness ratio of the beam. Beams which fail first in shear, assuming linear elastic behavior, have a lower energy/volume than those which fail in bending. Non-linear behavior and shear yielding add to the energy absorption capability of a beam. Additional deflection, tearing, yielding, etc. in beams beyond first failure (maximum load) contribute to the energy absorbed. These phenomena become increasingly important in thick beams where first failures are in shear. It is thus very difficult to compare behavior among materials using absorbed energy as a criterion unless they are tested at slenderness ratios representative of the intended application.

4. The tensile strength in bending exceeded the uniaxial tensile strength for the materials tested in this program when long slender beams were used. This phenomena is usually explained by size effects. On the other hand, less slender beams which appeared to fail in tension gave strengths lower than the uniaxial data. These results were explained by the fact that the shear stresses were near ultimate and thus caused some yielding and resultant redistribution of stresses. The results indicate that it is very difficult to obtain experimental values for uniaxial tensile strength from results of three point bend tests. Vice versa, it is difficult to predict the strength in bending based on uniaxial tension data, even when the bend specimen fails in outer fiber tension first.

Although bend tests are easy to perform, the results of this program indicate that bend test data must be analyzed and interpreted with great care if one wishes to deduce information on material behavior of composites. In particular, the application of the Charpy test as an impact resistance test for jet engine fan blade materials would require careful consideration of the effective slenderness ratio of the fan blade, careful choice of specimen geometry (thickness) and extensive interpretation of the resulting data.

REFERENCES

1. Prewo, K.M., "Development of Impact Resistant Metal Matrix Composites", AFML-TR-75-216, pg. 60-62, 1976.

2. Timoshenko, S., Strength of Materials: Part 1, D. Van Nostrand Co., Inc., New York, pg. 174, 1955.

3. Willis, J.R., "Hertzian Contact of Anisotropic Bodies", Journal of Mechanics and Physics of Solids, Vol. 14, 163-176, 1966.

4. Seely, F.B., Smith, J.O., Advanced Mechanics of Materials, John Wiley & Sons, Inc., New York, Article 109, 1966.

5. Timoshenko, S., Goodier, J.N., Theory of Elasticity, McGraw-Hill Book Company, New York, Article 23, 1951.

☆U.S.Government Printing Office: 1978 — 757-080/749